scientific reports

Check for updates

OPEN

A pilot study comparing three-dimensional models of tumor histopathology and magnetic resonance imaging

Anne Koivuholma[1,2]✉, Heli J. Sistonen[3], Katri Aro[1], Antti Mäkitie[1,5,6], Jaana Hagström[2,4,7] & Timo Atula[1,7]

Three-dimensional (3D) modeling is often used to provide better visual understanding. This has become an everyday tool especially in medical imaging. However, modeling soft tissue histopathology in 3D is in its early stages, thus making 3D comparison between radiology and histopathology difficult. Here, we sought to create a model that combines a model based on histopathological tumor borders and a model reformatted from magnetic resonance image (MRI). The 3D models were constructed from an oral squamous cell carcinoma (OSCC) resection specimen and a preoperative MRI scan. Potential challenges were identified, and respective solutions proposed. The 3D model based on histopathological tumor borders was constructed by a method that uses a 3D table scanner and modeling software. The 3D MRI model was constructed using 3D Slicer software. The two models were fitted together by anatomical landmarks in each model. We compared the volume and dimensions between the two 3D models. As a result, we created an image fusion that presents the soft-tissue resection specimen, its histopathological findings, and the MRI findings combined in a digital 3D form. Presenting these two 3D models within the resection specimen can serve as a tool to improve the multidisciplinary discussion of patient management. To create these models, only a few additional steps to a normal protocol are required.

Keywords Histopathology, Three-dimensional reconstruction, Computer aided design, Tongue, Radiology, Oral squamous cell carcinoma

Abbreviations

3D	Three-dimensional
OSCC	Oral squamous cell carcinoma
ADC	Apparent diffusion coefficient
MRI	Magnetic resonance imaging
CT	Computer tomography

Three-dimensional (3D) modeling has become an everyday tool in head and neck surgery that include bone resections and reconstruction models. Still, soft-tissue reconstructions, such as tumors, need further research to be modeled in 3D for clinical use. Soft tissue retraction and deformation after resection is not a new phenomenon but poses a challenge to new 3D modeling advancements[1–3]. Existing research shows publications of constructing a 3D printed mold, plate, or guide from preoperative magnetic resonance imaging (MRI) and then using it as a tool in tumor resection[4–7]. These methods have been applied mainly in prostate cancer. The Aforecited methods created the 3D tumor model solely from preoperative MRI. In common practice, the tumor

[1]Department of Otorhinolaryngology - Head and Neck Surgery, University of Helsinki and Helsinki University Hospital, P.O. Box 263, 00029 Helsinki, Finland. [2]Department of Pathology, HUSLAB, Helsinki University Hospital and University of Helsinki, Helsinki, Finland. [3]Department of Radiology, University of Helsinki and Helsinki University Hospital, Helsinki, Finland. [4]Department of Oral Pathology and Radiology, Institute of Dentistry, University of Turku, Turku, Finland. [5]Division of Ear, Nose and Throat Diseases, Department of Clinical Sciences, Intervention and Technology, Karolinska Institutet and Karolinska University Hospital, Stockholm, Sweden. [6]Research Program in Systems Oncology, Faculty of Medicine, University of Helsinki, Helsinki, Finland. [7]Jaana Hagström and Timo Atula shared senior authorship. ✉email: anne.koivuholma@helsinki.fi

margins are determined from histopathological analysis performed by the pathologist. Accordingly, more information on the tumor could be provided by presenting a 3D model from a histopathological perspective. In previous studies of prostate and breast cancer, 3D volumes have been reconstructed from preoperative MRI and whole-mount histopathology images slice-by-slice[8,9]. These methods are arduous and may not be applicable to other tissue types.

Understanding tumor orientation, topography, and exact site of where margins were determined is difficult after resection, especially in soft-tissue tumors due to their deformation. Image fusions have been proposed as a solution to address this problem and support interdisciplinary communication in planning patient care. An image fusion with MRI and computer tomography (CT) in oral squamous cell carcinoma (OSCC) has been presented[10–12], but to our knowledge image fusion with MRI and 3D histopathology in OSCC has not yet been offered.

In this study, we sought to create a 3D image fusion of an OSCC resection specimen, including histopathologically determined tumor borders within the specimen, and MRI-visualized tumor within the specimen. A recently published method of creating a histopathological 3D model was utilized[13], along with 3D Slicer and Fusion 360 software. Here, our aim was to develop a method to compare the findings of an MRI scan directly with the findings of histological slides in 3D models. This method allows the pathologist to choose freely the grossing directions (i.e., the directions from which the histopathology slides are made of) of the resection specimen, which means that the specimen can be processed in a normal manner. The method uses commonly available instruments and requires only a few additional steps. The image fusion created by this method could be used during the interdisciplinary discussion on the patient's postoperative care, allowing comparison of MRI findings to histopathology.

Materials and methods

Ethics approval and consent to participate

The Research Ethics Board of the Hospital District of Helsinki and Uusimaa approved the study protocol (record number: HUS/15/2024 approval date 7.2.2024, HUS/1092/2018 approval date 9.5.2018), and institutional permit was granted. An informed, written consent was obtained from the participant. We confirm that all experiments were performed in accordance with the Declaration of Helsinki.

Pilot case requirements

OSCC staging incorporates Stages 0-IV. The T classification for primary tumors is characterized by the diameter of the primary, depth of invasion and invasion to surrounding structures. The size of the primary ≥ 2 cm was agreed upon to ensure easier detection. We selected a typical, albeit large, tongue OSCC (classified as T3 clinically and pathologically) for developing the image fusion. The pilot case was required to have an MRI imaged with the hospital routine tumor protocol, with good visualization of the anatomic borders of the carcinoma, and with no significant artifacts. We chose MRI over CT as the imaging modality as MRI is the most widely used tool in diagnosing OSCC and can accurately evaluate the invasion in OSCC[14]. The MRI system was 1.5 T Siemens Avanto dot (Siemens Healthcare, Erlangen, Germany). We chose diffusion imaging for tumor segmentation as it most accurately differentiates malignant tissue from the surrounding reactive changes, thus not exaggerating the tumor size[15]. The diffusion images were obtained in axial plane with slice thickness of 4 mm using a readout-segmented echo-planar imaging sequence (RESOLVE). RESOLVE technique divides the k-space trajectory into multiple segments along the readout direction, reducing susceptibility artifacts, minimizing image distortion, and improving image quality for lesion detection and delineation. Diffusion imaging scanning parameters for RESOLVE sequence are provided in Table 1. A routine MRI tumor protocol was used, no additional sequences were needed. Diffusion weighting was applied in three orthogonal directions, using b-values of 50, 400, and 1000 s/mm^2. Apparent diffusion coefficient (ADC) map was calculated using all three b-values. The diffusion imaging stack of the lower neck was obtained using a single-shot echo-planar imaging technique. In addition to the diffusion images, the imaging protocol included axial T2 TSE, axial fat-saturated T2 TSE, axial T1 TSE, axial contrast-enhanced T1 TSE, axial fat-saturated contrast-enhanced T1, coronal contrast-enhanced T1 and coronal fat-saturated contrast-enhanced T1. The head and neck area was imaged in two sections: in the upper stack (including the face and upper neck), the slice thickness was 3 mm, to improve spatial resolution, and in the lower stack, the slice thickness was 4 mm. In the diffusion images, in the upper stack, which was used in

Slice direction	Axial/transverse
Slice thickness	4 mm
Intersection gap	0.8 mm
TR (time of repetitions)	4100 ms
TE (echo time)	61 ms
Field of view	227 × 250 mm^2
Matrix	140 × 154
Number of repetitions	1 (b = 50), 2 (b = 400), and 3 (b = 1000)
Time of acquisition	7 min 37 s
b-values	50, 400, and 1000 s/mm2

Table 1. Diffusion imaging scan parameters.

segmentation, the slice thickness was 4 mm, and in the lower stack, the slice thickness was 5 mm, for optimal signal-to-noise ratio.

3D model of tumor histopathology

In our previous study[13], we presented a novel method to demonstrate tongue OSCC histopathology in 3D[13]. This method created a 3D body of tumor outlines based on microscopy slides made from the resection specimen. The 3D tumor was presented within a 3D resection specimen, which was made by 3D scanning the specimen after resection. In this study, we used this method to create the 3D histopathology. The method involves using a 3D table scanner (Einscan SP, Shining 3D), Fusion 360 (v2023, Autodesk, Inc. Mill Valley, CA, USA) and Zen 3.0 (Carl Zeiss Microscopy GmbH, Oberkochen, Baden-Wurttemberg, Germany) software to create the model. Zen 3.0 is available free of charge, Fusion 360 is a commercial software that costs around $500 per year. In the operating room after the resection, pins were placed on to the resection specimen by the operating surgeon to mark the resection specimen orientation (anterior–posterior [A/P], cranial-caudal [C/C], left–right [L/R]) after which the resection specimen was measured and photographed in respective directions. After this, the pathologist examined the specimen by taking initial measurements and notes. Before formalin fixation, the resection specimen was scanned with a table scanner. The scanning took 15 min. To minimize soft tissue deformation, the resection specimen was placed on a special, albeit simple, rack during scanning, developed in our previous work[13]. After fixation, the pathologist sliced the resection specimen into microscopy slides and marked anatomical directions with tissue colors. The resection specimen slices were stained with hematoxylin eosin (H&E) staining according to standard protocol and microscopy slides of the slices were made. The pathologist drew the tumor outline onto the microscopy slides based on the H&E staining. Next, the sites of the slices were modelled using Fusion 360 into the scanned resection specimen. Then, the microscopy slides were scanned into a digital format and the tumor outline was drawn to the digitalized microscopy slides based on the outline previously drawn on the slide by the pathologist. These outlines were modelled by using Zen 3.0 into the digital resection specimen and further worked into a 3D model that presents the tumor histopathology as a 3D body inside the 3D tumor resection specimen.

3D model of tumor MRI

The 3D modeling software for MRI was required to export models in .stl form to be compatible with the 3D histopathology model. Multiple examples of constructing a 3D model of tumor MRI have been described[4–9,16]. We used tumor segmentation, as it is a simple and a relatively rapid method. 3D MRI segmentation has been used previously to depict tumor resection margins[17]. Software that met these requirements included 3D Slicer, InVesalius, ITK-Snap, and Seg3D. Based on an existing research, 3D shape error between the different software programs was shown to be insignificant[18]. When semi-automatic segmentation was used, a recent study showed InVesalius was the most accurate[19]. However, differentiating tumor tissue from the surrounding tongue muscle tissue cannot be performed accurately by automation, therefore segmentation had to be performed manually. 3D Slicer (https://www.slicer.org/) was selected as it is a free, open-source software, was perceived as the easiest to use, and can export the 3D model in .stl format[20].

The segmentation was performed manually by an experienced head and neck radiologist in our group (H.J.S. with 8 years of experience in ENT radiology). The tumor was manually segmented in diffusion trace-images (b-value 1000 s/mm^2), including only the areas that indicated restricted diffusion in ADC. The fat-saturated contrast-enhanced T1-weighted images and fat-saturated T2-weighted images aided in evaluating the tumor and surrounding anatomic structures, as these sequences have better spatial resolution. However, these sequences often exaggerate the lesion size as the surrounding edema can be difficult to differentiate from the actual tumor. In choosing the diffusion weighted images enabled the radiologist to segment the actual tumor borders and omit the inflamed zone around the tumor. The manual segmentation was performed primarily in the axial direction using the Segment Editor module in 3D Slicer. The software adjusted the segmentation in the coronal and sagittal reformations automatically. A 3D model was next created automatically by 3D Slicer's 3D function.

Fitting 3D histopathology and 3D MRI models together

After segmentation, the 3D MRI model was exported as an .stl file into 3D modeling software. Fusion 360 was selected as it can manage imported .stl files, is easy to use, and is affordable.

Our main challenge was orientating and fitting the models together. We addressed this problem by using anatomical checkpoints marked into both models at respective sites. With the 3D histopathological model, the 3D scan captured the resection specimen surface geometry sufficiently closely that the tongue centerline and pin markings indicating specimen orientation (A/P, C/C, and L/R) were visible in the finished scan. These served as anatomical checkpoints for the 3D histopathological model. For the 3D MRI model, these same orientational axes (A/P, C/C, and L/R) and the tongue centerline were marked into the segmentation in 3D Slicer using Segment Editor module. By orientating both 3D bodies according to A/P, C/C, and L/R axis and the tongue centerline, the two models could be fused together.

Results

A final model of the resection specimen, the histopathological tumor model, and the 3D tumor model derived from MRI data are presented in a digital 3D form (Fig. 1). Comparisons between histopathological and radiological model measurements in A/P, C/C, and L/R directions and 3D model volumes are presented in Table 2. These measurements were taken in Fusion 360 from the two 3D models. The 3D histopathological model dimensions were greater in L/R (11.2%) and C/C (9.0%) directions and smaller in A/P (49.6%) direction. The 3D histopathological tumor volume measured in Fusion 360 was 39.9% less than the 3D MRI model. Fusion 360 calculates the volume of the body by using the outline shell of the body. Comparisons between

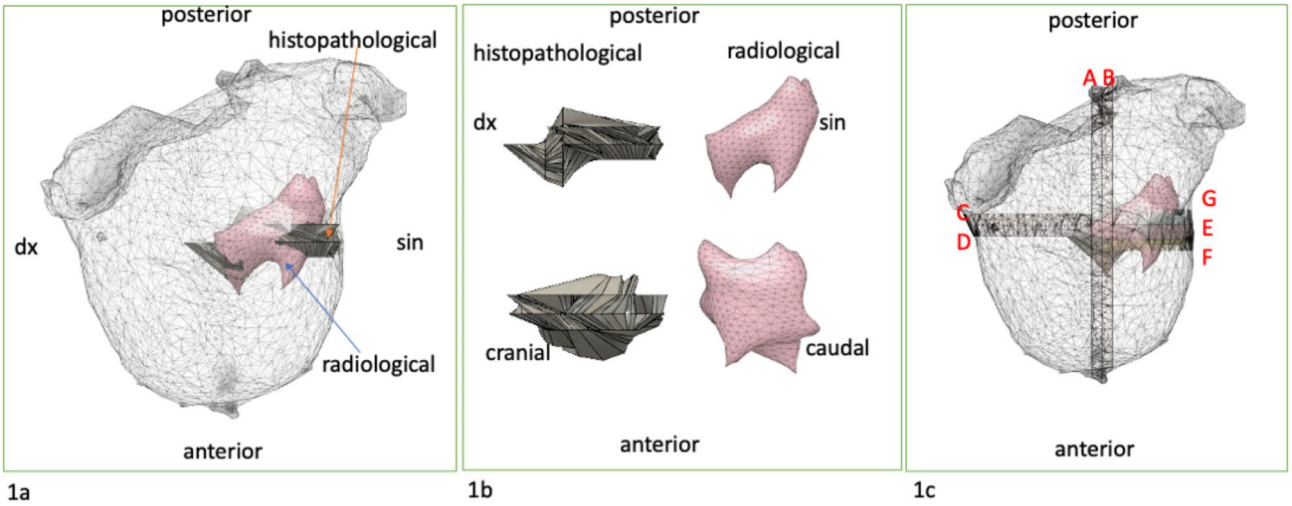

Fig. 1. (**a**) The resection specimen, histopathological, and radiological 3D model image fusion. (**b**) The histopathological and radiological 3D models side by side. (c) The sites of histological slices A-G.

Measurement	3D MRI model	3D histopathological model	Percent change MRI versus histopathology
Left/right (L/R) direction	3.35 cm	3.73 cm	− 11.3%
Anterior/posterior (A/P) direction	3.67 cm	1.85 cm	49.6%
Cranial/caudal (C/C) direction	3.01 cm	3.28 cm	− 9.0%
Volume	8.45 cm^3	5.08 cm^3	60.1%

Table 2. Dimension and volume comparison between histopathological and radiological model.

Measurement	Resection specimen after resection	Resection specimen after formalin fixation	Shrinkage
L/R direction	6.6 cm	7.0 cm	+ 6.1%
A/P direction	9.0 cm	7.7 cm	− 14.4%
C/C direction	4.6 cm	4.0 cm	− 13.0%

Table 3. Dimension comparison of resection specimen after resection and formalin fixation.

resection specimen measurements after resection and formalin fixation are presented in Table 3. The resection specimen was smaller in the A/P (14.4%) and C/C (13.0%) direction but larger in the L/R (6.1%) direction. All percentages were calculated by subtracting the MRI dimension or volume from the histopathological dimension or volume and divided by the MRI dimension or volume. An introductory video (Supplementary video S1) of the results, which includes an animation of hypothesized tumor deformation based on our findings, is available as supplemental material. A flow chart of a typical resection specimen processing with our additional steps is presented in Fig. 2.

Figure 1 was generated by Fusion 360 (v2023, Autodesk, Inc. Mill Valley, CA, USA, https://www.autodesk.com/products/fusion-360/overview?term=1-YEAR&tab=subscription) by the first author.

Discussion

In this study, we presented a novel 3D modeling method that shows a tongue OSCC resection specimen, the actual tumor, the sites of histological slices within the specimen, and the tumor MRI in a combined digital image fusion. Our method is suitable for soft-tissue specimens and allows the pathologist to choose the grossing direction of the resection specimen freely, meaning without predetermining the sites where to cut. Diffusion images or any other sequence with good visualization of the tumor can be used and no additional imaging is required. Our method combines the information of the tumor's histopathology and MRI into a single, easily understandable visual format that can be used e.g., in interdisciplinary discussion when planning the patient's postoperative evaluation and care. Presently, only a statement or a 2D image of tumor margins and a separate preoperative MRI are used to represent the tumor in clinical practice. Our method brings new benefits to current practice. Histopathological findings can be compared with the corresponding sites on the MRI scan and evaluation whether the MRI finding represents tumor tissue or not can be made. This method acts as feedback for surgeons, providing information on how the resected finding corresponds with the MRI. For example, for the

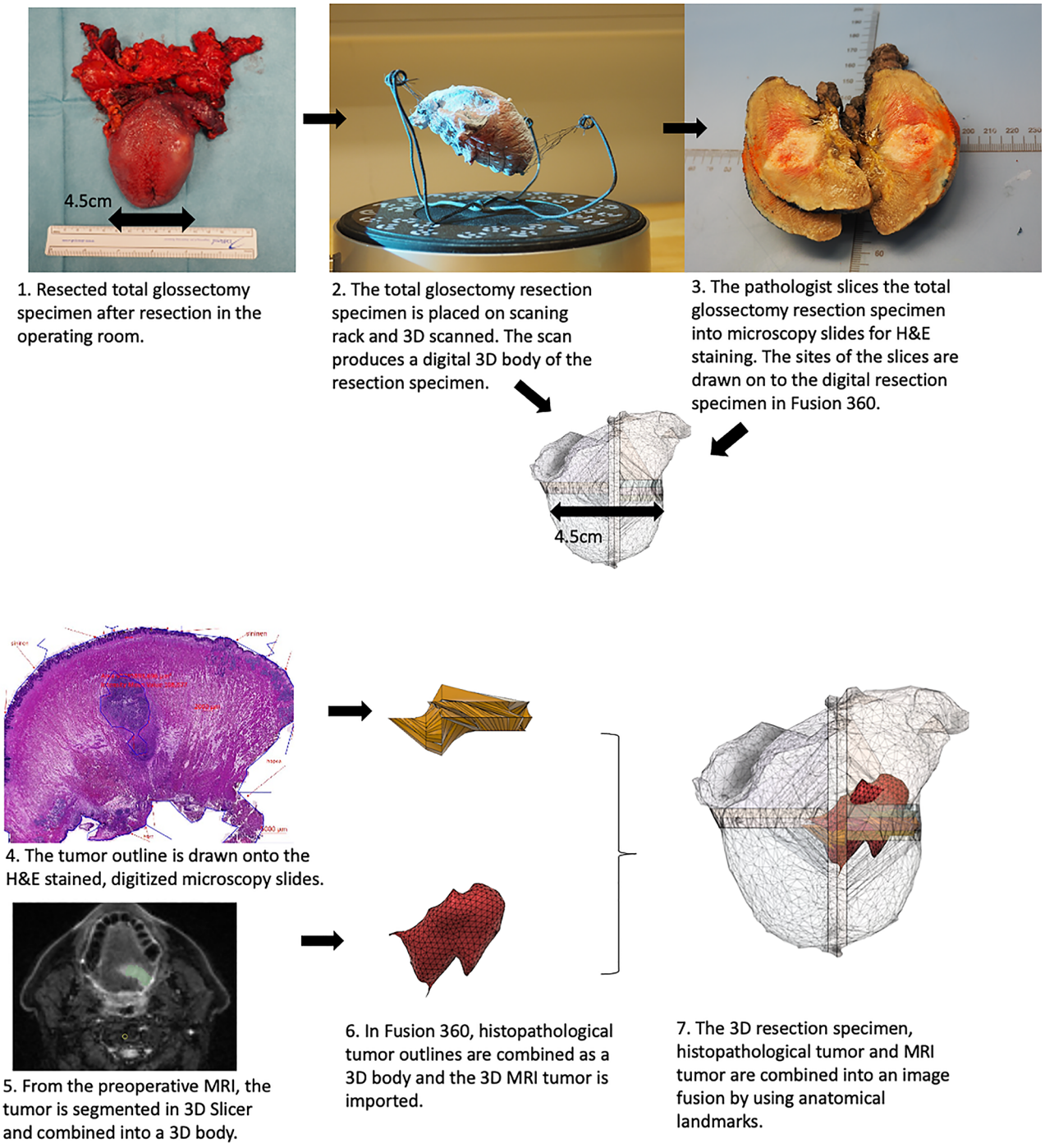

Fig. 2. Flowchart of the method.

surgeon, the exact sites of the tumor margins can be difficult to demonstrate using written pathology statement and 2D images. Comparing the tumor details between MRI and histopathology can be challenging, because the MRI sections on the stack are usually taken from a different angle than the histopathological section slides from the resection specimen. When they are both presented in 3D format provided with the anatomical reference of the resection specimen, the comparison is easier. Furthermore, if surgical margins remain inadequate and further surgery or intensified radiation therapy is considered, this method more precisely indicates the site of inadequate margins. This may help in planning additional treatment, as it shows the sites of tight margins in a more understandable, explicit way.

The greatest challenge when creating the 3D models was deformation of the soft-tissue specimen. In this case the resection specimen consisted of an entire tongue, which probably holds its shape better than a partial tongue resection. In our method, a special, but simple rack was used during scanning to preserve the resection specimen dimensions as well as possible. However, further development is needed to ensure that the shape is secured from

the moment the specimen is resected to the moment it is scanned, as this directly affects the comparability of the 3D scan to the 3D MRI.

Other challenges included fitting the MRI and histopathological 3D model together. In our study, the two 3D models were superimposed using anatomical landmarks. These landmarks were marked with pins in the histopathological model that determine the A/P and L/R axis. In the MRI model, the respective axes were drawn in the segmentation. As the patient underwent a total glossectomy in our pilot case, the tongue midline was easily identifiable in both models. Respective anatomical sites may be more difficult to identify e.g., when the resection specimen is smaller. In these cases, the corresponding anatomical landmark must be determined case by case.

Even though there appears to be both an increase and decrease in the dimensions after resection and formalin fixation, the volume comparison reveals that the histopathological model is only slightly smaller in volume than the MRI model. It is known that MRI often overestimates soft-tissue tumor invasion due to inflammation and edema around the tumor and in tongue-tumor artifacts produced by tongue movement[14,21–23]. Tissue shrinkage after resection is a known fact; the shrinkage rate of tongue OSCC specimens ranges from 7 to 20% after specimen removal from the patient[1,2,23]. In our model, the tumor volume difference was 3.4 cm^3 between the radiological and histopathological tumor and was thus slightly smaller. This figure includes shrinkage after resection and shrinkage due to formalin fixation. This difference can be caused by inaccuracies in measurements and not just by possible shrinkage. Another point to address is which model should be deemed as the more accurate. When creating the 3D MRI model, the tumor outline is known in every section made by the imaging. However, MRI overestimates the tumor outline[3,21–23]. The 3D histopathological model is derived from microscopically verified tumor outlines, but these outline sections are made only from sites relevant to the pathologist, not the entire tumor, hence the 3D model is an interpolation between these sections.

The steps required to create the 3D models of tumor histopathology and MRI by our method must be performed manually. One way of simplifying the process would be to automate the segmentation process from the MRI stack and the tumor border determination and 3D modeling from the microscopy slices. Ke et al.[3] described a method that uses deep learning to achieve segmentation in nasopharyngeal carcinoma MRI stacks. By developing this method further, the way resection specimens and margins are presented would ideally transform the pathology report in the future from a written statement to a visual, 3D statement including MRI findings.

When considering the aforementioned challenges, soft tissue deformation, shrinkage and MRI overestimation, the method can facilitate the comparison of the resection specimen's histopathological information and the tumor's MRI information in 3D format on a macroscopic level. However, this approach is not accurate enough to be used in a slice-by-slice or cellular-level comparison. The method needs further testing with greater number of OSCCs to determine the specificity in OSCC. The method was tested with only one case, which can be seen as a limitation as we present no repeatability of the method. The method needs to be tested with different tumors of different sizes to assess its applicability in general to tongue tumors. Also experience or training with modelling software is needed for the user to be able to use the method. Another limitation is that the tumor outline must be manually drawn both when segmenting the MRI as well as on the microscopy slides.

Conclusions

We developed a novel method of presenting tongue OSCC histopathology and MRI in a 3D digital image fusion. Compared to the traditional handling of tongue-tumor specimens, as an addition, our method requires only a table scanner, 3D modeling software, and a few additional steps to a normal protocol. To our knowledge, this is the first example of presenting soft-tissue histopathology and MRI comparison in 3D that allows normal handling and free grossing directions of the resection specimen. Our method may offer a valuable tool for interdisciplinary discussion when planning patient care and allows comparison of MRI findings with histopathology. The method requires prior training for the investigating pathologist or laboratory technician to be used in clinical setting. It also requires further testing with a variety of resection specimens to determine its applicability. In the future, automation and artificial intelligence are likely to provide solutions for reducing manual work and making our method even more applicable.

Data availability

All data generated or analyzed during the study are included in the published paper.

Received: 15 March 2024; Accepted: 3 January 2025
Published online: 13 January 2025

References

1. Goel, V. et al. Accuracy of MRI in prediction of tumour thickness and nodal stage in oral tongue and gingivobuccal cancer with clinical correlation and staging. *J. Clin. Diagn. Res.* **10**, TC01-05. https://doi.org/10.7860/JCDR/2016/17411.7905 (2016).
2. Johnson, R. E., Sigman, J. D., Funk, G. F., Robinson, R. A. & Hoffman, H. T. Quantification of surgical margin shrinkage in the oral cavity. *Head Neck* **19**, 281–286. https://doi.org/10.1002/(sici)1097-0347(199707)19:4%3c281::aid-hed6%3e3.0.co;2-x (1997).
3. Ke, L. et al. Development of a self-constrained 3D DenseNet model in automatic detection and segmentation of nasopharyngeal carcinoma using magnetic resonance images. *Oral Oncol.* **110**, 104862. https://doi.org/10.1016/j.oraloncology.2020.104862 (2020).
4. Priester, A. et al. Registration accuracy of patient-specific, three-dimensional-printed prostate molds for correlating pathology with magnetic resonance imaging. *IEEE Trans. Biomed. Eng.* **66**, 14–22. https://doi.org/10.1109/TBME.2018.2828304 (2019).
5. Darr, C. et al. Three-dimensional magnetic resonance imaging-based printed models of prostate anatomy and targeted biopsy-proven index tumor to facilitate patient-tailored radical prostatectomy-a feasibility study. *Eur. Urol. Oncol.* **5**, 357–361. https://doi.org/10.1016/j.euo.2020.08.004 (2022).

6. Jiang, W. et al. 3D-printed Model and guide plate for accurate resection of advanced cutaneous squamous cell carcinomas. *Front. Surg.* **9**, 964210. https://doi.org/10.3389/fsurg.2022.964210 (2022).
7. Dwivedi, D. K. et al. Development of a patient-specific tumor mold using magnetic resonance imaging and 3-dimensional printing technology for targeted tissue procurement and radiomics analysis of renal masses. *Urology* **112**, 209–214. https://doi.org/10.1016/j.urology.2017.08.056 (2018).
8. Sood, R. R. et al. 3D Registration of pre-surgical prostate MRI and histopathology images via super-resolution volume reconstruction. *Med. Image Anal.* **69**, 101957. https://doi.org/10.1016/j.media.2021.101957 (2021).
9. Mertzanidou, T. et al. 3D volume reconstruction from serial breast specimen radiographs for mapping between histology and 3D whole specimen imaging. *Med. Phys.* **44**, 935–948. https://doi.org/10.1002/mp.12077 (2017).
10. Thoenissen, P. et al. Image fusion improves interdisciplinary communication in the treatment of head and neck cancer. *J. Craniofac. Surg.* **33**, e439–e443. https://doi.org/10.1097/SCS.0000000000008447 (2022).
11. Kraeima, J. et al. Multi-modality 3D mandibular resection planning in head and neck cancer using CT and MRI data fusion: A clinical series. *Oral Oncol.* **81**, 22–28. https://doi.org/10.1016/j.oraloncology.2018.03.013 (2018).
12. Polfliet, M. et al. Registration of magnetic resonance and computed tomography images in patients with oral squamous cell carcinoma for three-dimensional virtual planning of mandibular resection and reconstruction. *Int. J. Oral. Maxillofac. Surg.* **50**, 1386–1393. https://doi.org/10.1016/j.ijom.2021.01.003 (2021).
13. Koivuholma, A. et al. Three-dimensional presentation of tumor histopathology: A model using tongue squamous cell carcinoma. *Diagnostics (Basel)* https://doi.org/10.3390/diagnostics11010109 (2021).
14. Li, M., Yuan, Z. & Tang, Z. The accuracy of magnetic resonance imaging to measure the depth of invasion in oral tongue cancer: A systematic review and meta-analysis. *Int. J. Oral. Maxillofac. Surg.* **51**, 431–440. https://doi.org/10.1016/j.ijom.2021.07.010 (2022).
15. Connolly, M. & Srinivasan, A. Diffusion-weighted imaging in head and neck cancer: Technique, limitations, and applications. *Magn. Reson. Imaging Clin. N. Am.* **26**, 121–133. https://doi.org/10.1016/j.mric.2017.08.011 (2018).
16. Giannitto, C. et al. Frozen section analysis and real-time magnetic resonance imaging of surgical specimen oriented on 3D printed tongue model to assess surgical margins in oral tongue carcinoma: Preliminary results. *Front. Oncol.* **11**, 735002. https://doi.org/10.3389/fonc.2021.735002 (2021).
17. Lorenzon, L. et al. 3D MRI segmentation and 3D circumferential resection margin evaluation for a standard rectal cancer assessment. *G Chir.* **39**, 152–157 (2018).
18. Kamio, T., Suzuki, M., Asaumi, R. & Kawai, T. DICOM segmentation and STL creation for 3D printing: A process and software package comparison for osseous anatomy. *3D Printing Med.* https://doi.org/10.1186/s41205-020-00069-2 (2020).
19. LoGiudice, A. et al. Assessment of the accuracy of imaging software for 3D rendering of the upper airway, usable in orthodontic and craniofacial clinical settings. *Progr. Orthod.* https://doi.org/10.1186/s40510-022-00413-8 (2022).
20. Fedorov, A. et al. 3D Slicer as an image computing platform for the Quantitative Imaging Network. *Magn. Reson. Imaging* **30**, 1323–1341. https://doi.org/10.1016/j.mri.2012.05.001 (2012).
21. Mao, M. H. et al. Accuracy of magnetic resonance imaging in evaluating the depth of invasion of tongue cancer. A prospective cohort study. *Oral. Oncol.* **91**, 79–84. https://doi.org/10.1016/j.oraloncology.2019.01.021 (2019).
22. Lam, P. et al. Correlating MRI and histologic tumor thickness in the assessment of oral tongue cancer. *AJR Am. J. Roentgenol.* **182**, 803–808. https://doi.org/10.2214/ajr.182.3.1820803 (2004).
23. Park, J. O. et al. Diagnostic accuracy of magnetic resonance imaging (MRI) in the assessment of tumor invasion depth in oral/oropharyngeal cancer. *Oral Oncol.* **47**, 381–386. https://doi.org/10.1016/j.oraloncology.2011.03.012 (2011).

Acknowledgements

The authors want to thank Derek Ho for proof-reading.

Author contributions

We are requesting shared senior authorship between J.H. and T.A. They have equally helped the first writer to complete her work and they have both worked hard to get it done. J.H. provided her expertise in developing the histopathological aspects of this work, whereas T.A. guided and conceptualized the surgical and radiological part of the work. Conceptualization, A.K., H.J.S., K.A., A.M., J.H. and T.A.; methodology, A.K., H.J.S., K.A. and T.A.; formal analysis, A.K. and H.J.S.; investigation, A.K., H.J.S., K.A., J.H. and T.A.; writing-original draft, prepared figures and tables, A.K.; writing-review & editing, A.K., H.J.S., K.A., A.M., J.H. and T.A.; resources, A.M.; funding acquisition A.K. and A.M.; supervision, T.A. All authors have read and agreed to the published version of the manuscript.

Funding

This study was supported by the Helsinki University Hospital Research Fund, Ida Montinin säätiö, Korvatautien tutkimussäätiö and Suomen Kulttuurirahasto. Open access funded by Helsinki University Library.

Declarations

Competing interests

The authors declare no competing interests.

Consent for publication

An informed, written consent was obtained from the participant to use images.

Additional information

Supplementary Information The online version contains supplementary material available at https://doi.org/10.1038/s41598-025-85478-1.

Correspondence and requests for materials should be addressed to A.K.

Reprints and permissions information is available at www.nature.com/reprints.

Publisher's note Springer Nature remains neutral with regard to jurisdictional claims in published maps and institutional affiliations.